Int J Thermophys (2008) 29:210–221
DOI 10.1007/s10765-007-0320-x

Evaluation of Cobalt–Carbon and Palladium–Carbon Eutectic Point Cells for Thermocouple Calibration

H. Ogura · M. Izuchi · M. Arai

Published online: 4 January 2008

Abstract Two cobalt–carbon (Co–C) eutectic point (1,324 °C) cells and one palladium–carbon (Pd–C) eutectic point (1,492 °C) cell were constructed for thermocouple calibration. The lengths of the Co–C and Pd–C cells were 297 mm, 140 mm, and 140 mm, respectively. The melting and freezing plateaux at the Co–C and Pd–C eutectic points were observed using Pt/Pd thermocouples. The repeatability of the plateau, the effect of the surrounding temperature, and the temperature profile in the cell were measured, and the heat flux effect along the thermometer well was evaluated. When the plateaux of Co–C (297 mm height), Co–C (140 mm height), and Pd–C cells, were measured three times, seven times, and six times, respectively, the standard deviations of the melting points were 0.1 μV, 0.1 μV, and 0.4 μV, respectively. According to the temperature profiles along the thermometer well during the melting plateaux, it was found that the Pt/Pd thermocouple should be inserted at least 9.5 cm, 5 cm, and 6 cm below the surface of the eutectic alloys in the Co–C (297 mm height), Co–C (140 mm height), and Pd–C cells with the furnace set-point 16 °C above the melting point.

Keywords Calibration · Cobalt–carbon eutectic point · Palladium–carbon eutectic point · Pt/Pd thermocouple

H. Ogura (✉) · M. Izuchi (✉) · M. Arai (✉)
National Metrology Institute of Japan (NMIJ), AIST, Central 3, 1-1-1 Umezono, Tsukuba, Ibaraki, Japan
e-mail: h.ogura@aist.go.jp

M. Izuchi
e-mail: m.izuchi@aist.go.jp

M. Arai
e-mail: masaru-arai@aist.go.jp

1 Introduction

Thermocouples are widely used in industry to measure high temperatures. However, it is well known that their emf drifts when exposed to high temperatures, thereby compromising their calibration. To accurately monitor the drifts, a stable fixed point or a stable thermometer is usually used as a reference. Several institutes reported measurements of the drifts of Pt/Pd thermocouples at metal-fixed points below 1,100 °C [1–5]. In the temperature range from 1,100 °C to 1,550 °C (from the copper point at 1,084.62 °C to the palladium point at 1,554.8 °C), the drifts of the thermocouples were investigated using a radiation thermometer as the reference [1,6], due to the lack of practical fixed points above 1,100 °C. Generally, it is difficult to calibrate a thermocouple with a radiation thermometer. A practical fixed point above 1,100 °C would be a more suitable reference to accurately evaluate the emf drift and to calibrate thermocouples in that range.

As recently reported, the metal–carbon eutectic points are practical reference points for the calibration of thermocouples [7]. Measurements of the eutectic points of iron–carbon (Fe–C, 1,153 °C), cobalt–carbon (Co–C, 1,324 °C), nickel–carbon (Ni–C, 1,329 °C), palladium–carbon (Pd–C, 1,492 °C), platinum–carbon (Pt–C, 1,738 °C), and ruthenium–carbon (Ru–C, 1,953 °C) by means of Type R, Type S, Type B, Pt/Pd, and W–Re thermocouples have been reported [8–11]. However, since it is difficult to construct a large-scale eutectic point cell with a long thermometer well, the heat flux effect along the thermometer well has been insufficiently investigated. There is no doubt that the evaluation of the heat flux effect is essential for accurate thermocouple calibration, because heat will easily leak along the thermometer well and the thermocouple itself such that the thermocouple may not reach the temperature of the eutectic phase transition.

In this work, cells were constructed for thermocouple calibrations at the Co–C and Pd–C eutectic points. The repeatability of the melting and freezing plateaux, the influence of the surrounding temperature, and the temperature profile along the thermometer well were measured using Pt/Pd thermocouples. We focused especially on the measurements of the temperature profile, since they included information concerning the heat flux along the thermometer well.

2 Measurements

2.1 Measurement Setup

To accurately measure the emf of the thermocouple at the eutectic fixed points, a vertical electric furnace constructed in our institute was used. The furnace and the cell are illustrated in Fig. 1. The assembly consists of one main heater, two end heaters, and an open cell made of high-purity alumina. The open alumina cell includes graphite wool, graphite disks, and a metal–carbon cell. Two open alumina cells were prepared, one for the Co–C eutectic point and one for the Pd–C eutectic point. These were filled with argon gas maintained at a pressure of approximately 110 kPa to prevent the flow of ambient air into the tube. The thermometer well was a high-purity alumina protection tube (7 mm outer diameter, 5 mm inner diameter, 680 mm length) closed at one end.

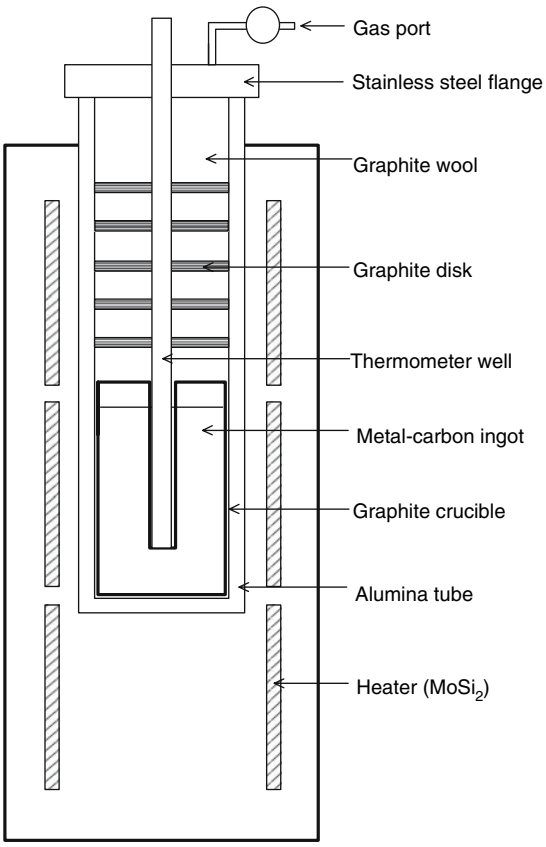

Fig. 1 Schematic diagram of the eutectic point cell and furnace

The dimensions of the crucibles "Cell-A" and "Cell-B" are shown in Fig. 2. Both crucibles are made from high-purity graphite (99.9995 %) having an outer diameter of 46 mm, and heights of 297 mm and 140 mm for Cell-A and Cell-B, respectively. To minimize the likelihood of cracking of the crucible, C/C (carbon fiber reinforced carbon composite) sheets were set between the sleeve and the outer crucible as a buffer [12]. Graphite sheets were set inside the graphite well to prevent sticking of the thermometer well in case of leakage of metal from the crucible.

All graphite crucibles were baked at 1,500 °C for 3 h in argon gas before filling with cobalt shots, palladium powder, and carbon powder. For the two Co–C eutectic cells, graphite crucibles Cell-A and Cell-B were filled with pure cobalt shot mixed with graphite powder of high purity (99.9999 %) at approximately the eutectic composition. These were labeled $Co–C_{(Cell\text{-}A)}$ and $Co–C_{(Cell\text{-}B)}$, respectively. The nominal purity of the cobalt shot was 99.999 % (Nippon Mining & Metals Co., Ltd.) and was supplied in the form of 1.5 mm cubes. For the Pd–C cell, the graphite crucible Cell-B was filled with pure palladium powder mixed with graphite powder of high purity (99.9999 %) at approximately the eutectic composition, and this was labeled $Pd–C_{(Cell\text{-}B)}$. The nominal purity of the palladium was 99.999 % (Ishifuku Metal

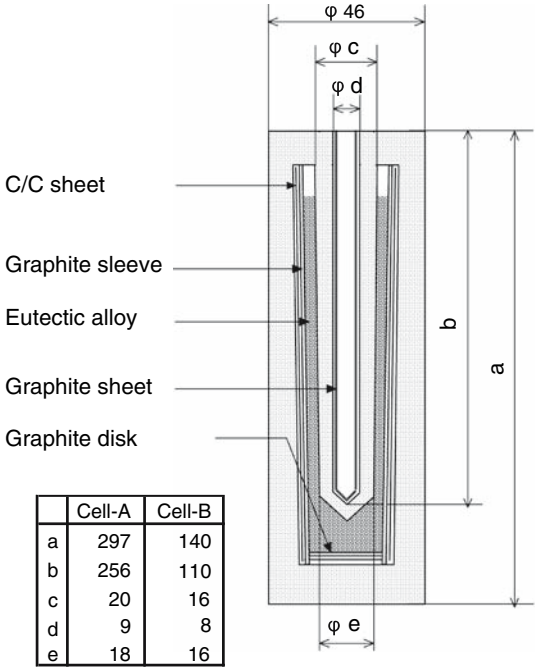

	Cell-A	Cell-B
a	297	140
b	256	110
c	20	16
d	9	8
e	18	16

Fig. 2 Dimensions of the eutectic point cells

Industry Co., Ltd.). The crucible and its content were heated until the content completely melted at the eutectic melting point under argon atmosphere, and then cooled to room temperature. This process was repeated until the crucible was fully filled with alloy ingot, which took four to six fillings depending on the crucible and metal. After filling, the $Co–C_{(Cell\text{-}A)}$, $Co–C_{(Cell\text{-}B)}$, and $Pd–C_{(Cell\text{-}B)}$ eutectic cells contained 430 g, 170 g, and 220 g of eutectic alloys, and the surface of the alloy ingot, $d_{surface}$, was at a height of 175 ± 12 mm, 100 ± 5 mm, and 85 ± 3 mm from the bottom of the graphite wells, respectively. The uncertainty of the position is attributed to an uneven surface shape of the eutectic alloy due to the high viscosity.

2.2 Preparation of Pt/Pd Thermocouples

To measure the Co–C and Pd–C eutectic points, three Pt/Pd thermocouples labeled TC-co-a, TC-co-b, and TC-pd-b were used. They were constructed following the procedure reported by Burns et al. [1]. The diameter of both the Pt and Pd wires was 0.5 mm. The outside diameter of the twin-bore alumina tube was 4 mm, the bore was 1.2 mm diameter, and the length was 700 mm. To avoid a large emf drift [13], thermocouples TC-co-a and TC-co-b were exposed to the Co–C eutectic point for 300 h, and the thermocouple TC-pd-b was exposed to the Pd–C eutectic point for 300 h. The emf at the eutectic point was measured automatically using a digital multimeter (Fluke 8508A). The reference junction was held in a water bath (Hart Scientific 7312) maintained at 0.02 °C to avoid the freezing of water inside the bath. After the measurements,

the data were corrected to 0 °C. During the determinations of the repeatability and the influence of the surrounding temperature, the measuring junction of the thermocouple was held 1 cm above the bottom of the graphite well.

3 Results

3.1 Results for Cell Type A

3.1.1 Repeatability of Cell Type A

The melting and freezing plateaux at the Co–C eutectic point obtained from measurements using the thermocouple TC-co-a are shown in Fig. 3. The heating and cooling patterns were stepwise temperature changes from below the melting point to above it and vice versa, respectively. The temperature difference between the surroundings T_{surround} and the melting point T_{melt}, $|T_{\text{surround}} - T_{\text{melt}}|$, was 2 °C. As the stability of the furnace was within 0.3 °C during these measurements, the uncertainty of the temperature offset $|T_{\text{surround}} - T_{\text{melt}}|$ is 0.3 °C.

Figure 3 illustrates the three melting and freezing plateaux that were measured. The slight difference of the plateau lengths arises from the uncertainty of the temperature offset $|T_{\text{surround}} - T_{\text{melt}}|$. The emf for the melting point was determined at the inflection point of the melting plateau, while that for the freezing point was taken at the peak of the plateau soon after recalescence from the supercool. Both melting and freezing points reproduced within ±0.2 μV, with standard deviations of 0.1 μV. The change of 0.2 μV in the emf of the Pt/Pd thermocouple at the Co–C eutectic point was equivalent to 8.5 mK.

3.1.2 Effect of Surrounding Temperature on Cell Type A

Figure 4 shows the effect of the surrounding temperature as determined by changing the temperature setting above or below the melting point $|T_{\text{surround}} - T_{\text{melt}}|$. All heating and cooling patterns were stepwise temperature changes. The temperature settings

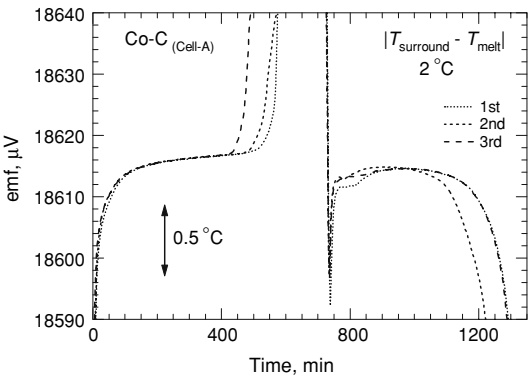

Fig. 3 Melting and freezing plateaux of the Co–C(Cell-A) cell. Number in the legend shows the order of runs

were 16 °C, 8 °C, 4 °C, 2 °C, and 1 °C, at which each plateau was measured thrice using the thermocouple TC-co-a. As the magnitude of the temperature offset from the phase transition increases, the melting point shows an approximately constant value, but the freezing point has a tendency to decrease.

3.1.3 Temperature Profile for Cell Type A

Figure 5 shows the temperature profiles along the thermometer well during melting when the temperature settings were 16 °C, 8 °C, 4 °C, 2 °C, 1 °C, and 0 °C different from that of the phase transition. Heating and cooling patterns for these 16 °C, 8 °C, 4 °C, 2 °C, and 1 °C temperature offsets were essentially stepwise temperature changes. The temperature offset of 0 °C was obtained by changing the temperature offset from 1 °C to 0 °C just after the measurement of the temperature profile with an offset of 1 °C. The ordinate shows the temperature difference ΔT from 1 cm above the bottom of the graphite well, and the abscissa shows the position d of the thermocouple above the bottom of graphite well. The vertical broken line shows the height of the surface of the eutectic alloy. The thermocouple TC-co-a was moved upwards from $d = 1$ cm to $d = 25$ cm at a rate of $2.2\,\mathrm{cm} \cdot \mathrm{min}^{-1}$.

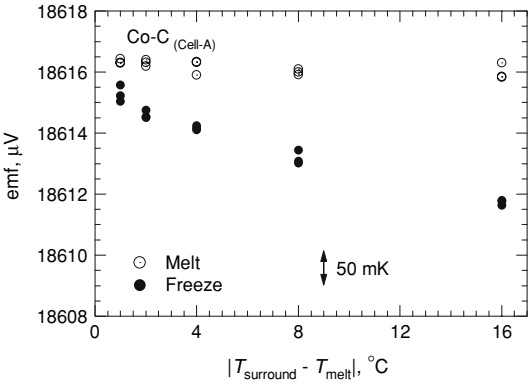

Fig. 4 Effect of surrounding temperature on the $\mathrm{Co–C}_{(\mathrm{Cell\text{-}A})}$ cell

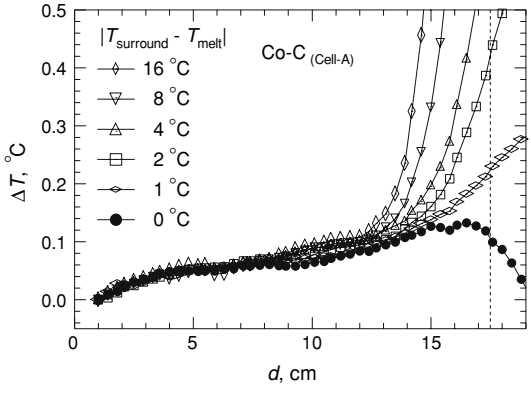

Fig. 5 Temperature profiles along the thermometer well of the $\mathrm{Co–C}_{(\mathrm{Cell\text{-}A})}$ cell during melting

All temperature profiles show the same tendency to increase at a constant rate of $0.01\,\mathrm{K}\cdot\mathrm{cm}^{-1}$ from 1 cm to 8 cm above the bottom of graphite well. This means that the temperature profile for this region was independent of change in the surrounding temperatures.

3.2 Results for Cell Type B

3.2.1 Repeatability of Cell Type B

The melting and freezing plateaux of Co–$C_{(\mathrm{Cell\text{-}B})}$ and Pd–$C_{(\mathrm{Cell\text{-}B})}$ cells obtained from measurements using thermocouple TC-co-b and TC-pd-b, respectively, are shown in Fig. 6a and b. The furnace temperature offset from the melting point, $|T_{\mathrm{surround}} - T_{\mathrm{melt}}|$, was 4 °C. As the stabilities of the furnace during the Co–C and Pd–C measurements were within 0.3 °C and 0.7 °C, the uncertainties of the temperature offset $|T_{\mathrm{surround}} - T_{\mathrm{melt}}|$ are 0.3 °C and 0.7 °C, respectively. The plateaux at the Co–C and Pd–C eutectic points were measured seven and six times, respectively. In Fig. 6a, the melting and freezing points of the Co–$C_{(\mathrm{Cell\text{-}B})}$ cell reproduced within $\pm 0.2\,\mu\mathrm{V}$ and $\pm 0.8\,\mu\mathrm{V}$, with standard deviations of $0.1\,\mu\mathrm{V}$ and $0.3\,\mu\mathrm{V}$, respectively. On the other hand, in Fig. 6b, the melting and freezing points of the Pd–$C_{(\mathrm{Cell\text{-}B})}$ cell

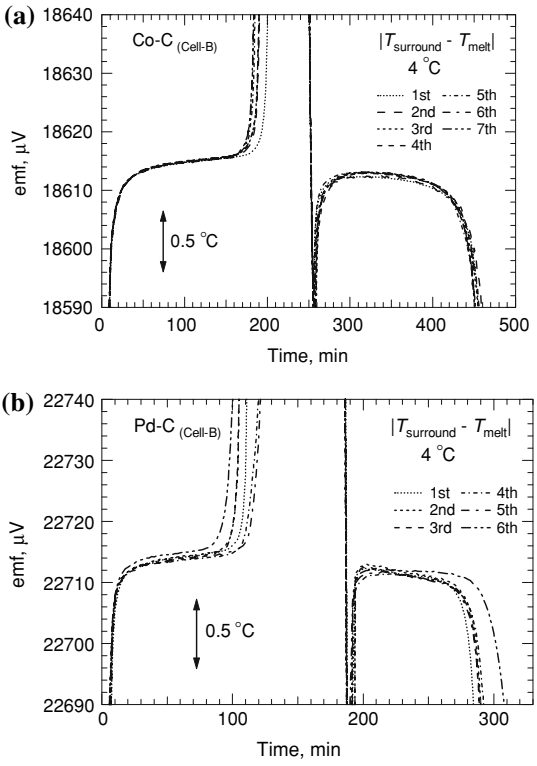

Fig. 6 Melting and freezing plateaux of (**a**) Co–$C_{(\mathrm{Cell\text{-}B})}$ and (**b**) Pd–$C_{(\mathrm{Cell\text{-}B})}$. Numbers in the legends show the order of runs

reproduced within $\pm 1.2\,\mu V$ and $\pm 1.4\,\mu V$, with standard deviations of $0.4\,\mu V$ and $0.5\,\mu V$, respectively. The change of $1.2\,\mu V$ in the emf of the Pt/Pd thermocouple at the Pd–C eutectic point was equivalent to 48 mK.

3.2.2 Effect of Surrounding Temperature on Cell Type B

Figure 7a and b show the influence of the surrounding temperature on the $Co–C_{(Cell\text{-}B)}$ and $Pd–C_{(Cell\text{-}B)}$ cells for temperature offsets of 16 °C, 8 °C, 4 °C, 2 °C, and 1 °C. Except for seven times when the temperature offset was 4 °C to establish the repeatability, the plateaux of the $Co–C_{(Cell\text{-}B)}$ cell were measured once at each temperature offset. The plateaux of the $Pd–C_{(Cell\text{-}B)}$ cell were measured four times at temperature offsets of 16 °C and 8 °C, and six times, seven times, and twice at temperature offsets of 4 °C, 2 °C, and 1 °C, respectively. As the temperature offset increases, the melting points show approximately constant values, but the freezing points have a tendency to decrease.

3.2.3 Temperature Profile for Cell Type B

Figure 8a and b show the temperature profiles along the thermometer wells for the $Co–C_{(Cell\text{-}B)}$ and $Pd–C_{(Cell\text{-}B)}$ cells during melting, when the temperature offsets

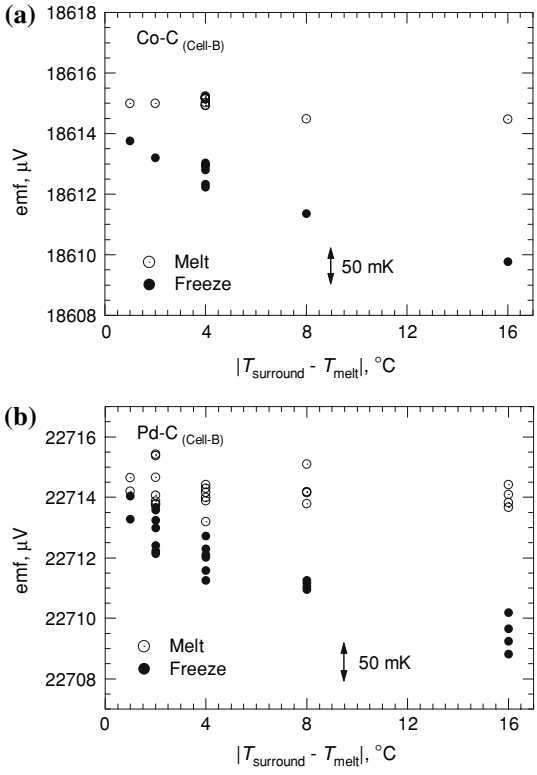

Fig. 7 Effect of surrounding temperature on (**a**) $Co–C_{(Cell\text{-}B)}$ and (**b**) $Pd–C_{(Cell\text{-}B)}$

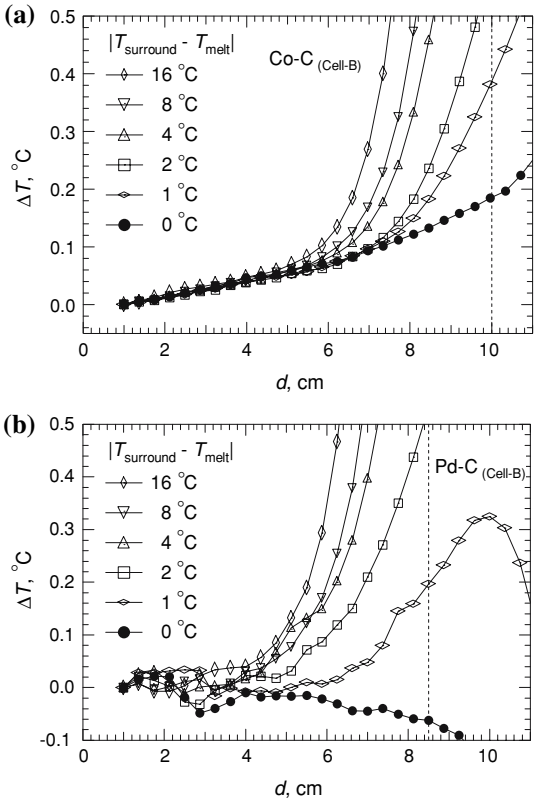

Fig. 8 Temperature profiles along the thermometer well of (**a**) Co–$C_{(Cell\text{-}B)}$ and (**b**) Pd–$C_{(Cell\text{-}B)}$ during melting

were 16 °C, 8 °C, 4 °C, 2 °C, 1 °C, and 0 °C. The vertical broken line shows the height of the surface of the eutectic alloy. The thermocouple was moved upwards 24 cm from a height of 1 cm above the bottom of the graphite well at a rate of $2.2\,cm \cdot min^{-1}$. The temperature profile of the Co–$C_{(Cell\text{-}B)}$ cell has a tendency to increase at a constant rate of $0.01\,K \cdot cm^{-1}$ from 1 cm to approximately 5 cm above the bottom of the graphite well at a constant rate of $16\,mK \cdot cm^{-1}$. The temperature profile of the Pd–$C_{(Cell\text{-}B)}$ cell shows a nearly constant value from 1 cm to approximately 4 cm above the bottom of the graphite well. This means that the temperature profile in this region was independent of change in the surrounding temperature.

4 Discussion

The times required to measure the temperature distribution of Co–$C_{(Cell\text{-}A)}$, Co–$C_{(Cell\text{-}B)}$, and Pd–$C_{(Cell\text{-}B)}$ cells from the bottom of well to the surface of alloy were 8 min, 5 min, and 4 min, respectively. These time intervals were short enough compared to the time for complete melting. Therefore, the temperature distribution measurement can be considered an adequate representation of the actual temperature distribution within the cell. Furthermore, as described in Figs. 5, 8a, and b, there are

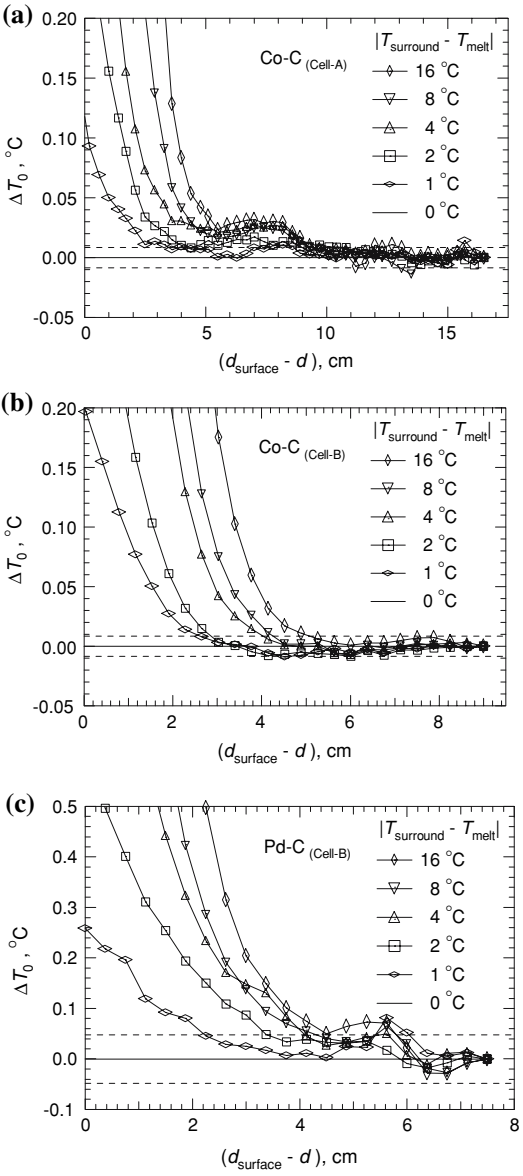

Fig. 9 Heat flux effect along the thermometer well on (**a**) Co–$C_{(Cell\text{-}A)}$, (**b**) Co–$C_{(Cell\text{-}B)}$, and (**c**) Pd–$C_{(Cell\text{-}B)}$ cell during melting

regions where the temperature profiles change at constant rates ($K \cdot cm^{-1}$) unaffected by the surrounding temperature change. These regions of nearly constant temperature grew in extent as the temperature offset decreased, and approached the surface of the alloy when the temperature offset became 0 °C. This shows that a solid–liquid interface adequately surrounded the thermocouple over nearly the entire length of the alloy during the measurement of the temperature distributions shown in Figs. 5, 8a, and b.

Figure 9a–c show the temperature differences of the temperature profile at various temperature offsets with respect to the profile at 0 °C temperature offset, ΔT_0. This

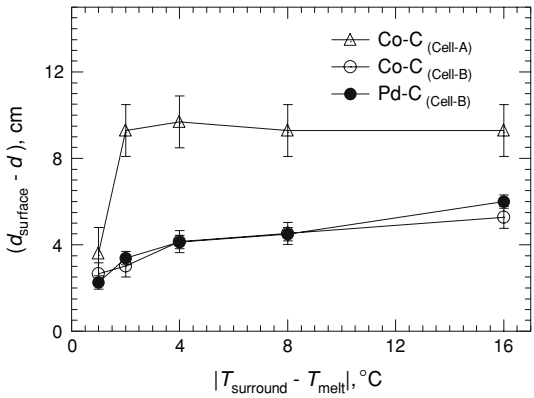

Fig. 10 Immersed length of the thermocouple from the surface of the eutectic alloy to the region independent of change in the surrounding temperature. Error bars are attributed to an uneven surface of the eutectic alloy due to the high viscosity

difference shows the influence of the heat flux along the thermometer well during the melting of the eutectic alloy. To represent this effect more clearly, the abscissa ($d_{\text{surface}} - d$) shows the immersion depth from the surface of the eutectic alloy. The horizontal broken lines in Fig. 9a–c show the repeatability of ± 8.5 mK, ± 8.5 mK, and ± 48 mK obtained from the melting points in Figs. 3, 6a, and b, respectively. As the immersion depth increases, a region where ΔT_0 is within the repeatability appears. This means that, within this region, the temperature is independent of the influence of heat flux.

Figure 10 shows the immersion depth from the surface of the eutectic alloy to the region independent of the influence of the heat flux for temperature offsets of 16 °C, 8 °C, 4 °C, 2 °C, and 1 °C. The uncertainty of the position is attributed to an uneven surface shape of the eutectic alloy due to the high viscosity as described in Sect. 2.1. When the temperature offset above the melting point is 16 °C, the Pt/Pd thermocouple should be inserted at least 9.5 cm from the surface of the eutectic alloy in the Co–$C_{(\text{Cell-A})}$ cell so that a melting point measurement independent of the heat leakage along the thermometer well of the cell can be obtained. On the other hand, to obtain a melting point that is independent of the influence of the heat flux for the Co–$C_{(\text{Cell-B})}$ and Pd–$C_{(\text{Cell-B})}$ cells, the Pt/Pd thermocouple should be inserted at least 5 cm and 6 cm, respectively, below the surface of the eutectic alloys for an offset of 16 °C. In other words, when the Co–C and Pd–C eutectic points are to be realized using Co–$C_{(\text{Cell-A})}$, Co–$C_{(\text{Cell-B})}$, and Pd–$C_{(\text{Cell-B})}$ cells with a 16 °C furnace offset, the thermocouple should be positioned more than 9.5 cm, 5 cm, and 6 cm, respectively, below the surface of the eutectic alloy. Since the temperature offset reflects the heat flux, the mentioned thermocouple positions represent the condition required to obtain freezing point measurements unaffected by the heat flux for a temperature offset of 16 °C below the melting point.

Since the thermocouples were held at 16.5 cm, 9 cm, and 7.5 cm below the surface of the eutectic alloys in the Co–C $_{(\text{Cell-A})}$, Co–$C_{(\text{Cell-B})}$, and Pd–$C_{(\text{Cell-B})}$ cells as shown in Figs. 5, 8a, and b, respectively, the melting and freezing points measured in the present study are free from the influence of heat leakage. Accordingly, the tendency of the freezing point to decrease with an increase in the temperature offset, as shown

in Figs. 4, 7a, and b, should not be due to the influence of heat leakage, but from the influence on the freezing rate or other factors.

5 Summary

The Co–$C_{(Cell-A)}$, Co–$C_{(Cell-B)}$, and Pd–$C_{(Cell-B)}$ cells were constructed to realize the metal–carbon eutectic points, and the melting and freezing plateaux of these cells were evaluated using Pt/Pd thermocouples. The heating and cooling patterns were stepwise temperature changes from temperatures below the melting point to above it, and vice versa. The repeatability of the plateau and the influence of the surrounding temperature were determined. When the temperature offsets from the melting points of Co–$C_{(Cell-A)}$, Co–$C_{(Cell-B)}$, and Pd–$C_{(Cell-B)}$ cells were 2 °C, 4 °C, and 4 °C, the standard deviations of the melting points were 0.1 μV, 0.1 μV, and 0.4 μV, respectively.

Temperature profiles along the thermometer well were evaluated during the melting plateaux. It was found that the surface of the eutectic alloys in the Co–$C_{(Cell-A)}$, Co–$C_{(Cell-B)}$, and Pd–$C_{(Cell-B)}$ cells should be more than 9.5 cm, 5 cm, and 6 cm, respectively, above the bottom of the graphite well when the temperature offset from the melting point was 16 °C.

For an accurate thermocouple calibration, the evaluation of heat leakage is important. The investigation of the heat flux effect from this experiment will be useful in evaluating the uncertainty of thermocouple calibrations at the Co–C and Pd–C eutectic points.

Acknowledgment The authors are indebted to Mr. Yamada of the Radiation Thermometry Section, NMIJ/AIST, for his valuable assistance during the construction of the eutectic point cells used in the present work.

References

1. G.W. Burns, D.C. Ripple, M. Battuello, Metrologia **35**, 761(1998)
2. F. Edler, M. Nau, *Proceedings of EUROMET Workshop Temperature* (Paris, 1998), pp. 85–89
3. G.W. Burns, D.C. Ripple, in *Proceedings of TEMPMEKO 2001, 8th International Symposium on Temperature and Thermal Measurements in Industry and Science*, ed. by B. Fellmuth, J. Seidel, G. Scholz (VDE Verlag, Berlin, 2002), pp. 61–66
4. K.D. Hill, Metrologia **39**, 51 (2002)
5. H. Ogura, H. Numajiri, K. Yamazawa, J. Tamba, M. Izuchi, M. Arai, in *Temperature: Its Measurement and Control in Science and Industry*, vol. 7, ed. by D. C. Ripple (AIP, New York, 2003), pp. 485–489
6. M. Battuello, *Proceedings of EUROMET Workshop Temperature* (Paris, 1998), pp. 107–112
7. E.R. Woolliams, G. Machin, D.H Lowe, R. Winkler, Metrologia **43**, R11 (2006)
8. Y. Yamada, F. Sakuma, A. Ono, Metrologia **37**, 71 (2000)
9. R. Morice, M. Megharfi, J.-O. Favreau, E. Morel, I. Didialaoui, J.-R. Filtz, *Proceedings of TEMPMEKO 2004, 9th International Symposium on Temperature and Thermal Measurements in Industry and Science*, ed. by D. Zvizdić, L.G. Bermanec, T. Veliki, T. Stašić (FSB/LPM, Zagreb, Croatia, 2004), pp. 847–852
10. F. Edler, A.C. Baratto, Metrologia **42**, 201 (2005)
11. Y. Kim, I. Yang, S.Y. Kwon, K.S. Gam, Metrologia **43**, 67 (2006)
12. Y. Yamada, B. Khlevnoy, Y. Wang, T. Wang, K. Anhalt, Metrologia **43**, S140 (2006)
13. H. Ogura, K. Yamazawa, M. Izuchi, M. Arai, *Proceedings of TEMPMEKO 2004, 9th International Symposium on Temperature and Thermal Measurements in Industry and Science*, ed. by D. Zvizdić, L. G. Bermanec, T. Veliki, T. Stašić (FSB/LPM, Zagreb, Croatia, 2004), pp. 459–464